RSC Advances

ROYAL SOCIETY OF CHEMISTRY

www.rsc.org/advances

Cite this: DOI: 10.1039/c0xx00000x

www.rsc.org/xxxxxx

ARTICLE TYPE

Organic – Inorganic Nanohybrids and their applications in Silver Extraction, Chromogenic Cu^{2+} detection in Biological Systems, and Hemolytic Assay

Ajnesh Singh[a], Vimal Kumar Bhardwaj[a], Gurinder Kaur[b], Kamalpreet Kaur[a], Narinder Singh[a,*],Mandeep Singh Bakshi[c,*]

Received (in XXX, XXX) Xth XXXXXXXXX 20XX, Accepted Xth XXXXXXXXX 20XX
DOI: 10.1039/b000000x

Fluorescent organic nanoparticles (FONPs) were prepared from an organic tripodal Schiff base ligand (OTL) in pure water by implementing the re-precipitation method. FONPs were perfectly spherical in shape and their size increased with the increase in the amount of OTL. Bigger FONPs were more fluorescent than the smaller ones and their fluorescent emission showed strong temperature dependence due to their amorphous nature. They demonstrated specific binding towards Ag^{+} ions which resulted in strong reducing ability from Ag(I) to Ag(0) to produce organic – inorganic hybrid nanoparticles (i.e. Ag@FONPs). FONPs and Ag@FONPs were characterized by UV-visible, fluorescence, transmission electron microscopic (TEM), NMR, IR, and XRD studies. We showed that the FONPs can be repeatedly used for the extraction of Ag in a systematic manner, while Ag@FONPs can be used for the chromogenic detection of Cu^{2+} in biological systems even in the presence of other metal ions. A detailed haemolytic analysis demonstrated that the smaller Ag@FONPs can also be suitable drug release vehicles in systematic circulation in comparison to the bigger ones.

Introduction

Several pharmaceutical and consumer products develop a range of organic compounds for their diverse use. To improve the performance of organic products especially in aqueous phase while keeping the environmental concerns in consideration, researchers use formulations with surfactants, other composite mixtures, and surface decoration. Conversion of organic compounds into organic nanoparticles (ONPs) dramatically increases their applications in diverse environments including biological systems due to their interesting medicinal, electronic, and optical properties.[1-5] Fluorescent organic nanoparticles (FONPs) are known to have marked improved optical and photo-physical properties than their parent organic molecules, and hence can be used as chemosensors for the detection of biologically important ions, biomolecules, molecular imaging probes etc.[6-9] Recently, Petkau *et al* reported the controlled bifunctionalization of fluorescent π-conjugated oligomer nanoparticles, which is a novel approach with high applicability to multi-targeted imaging and sensing in biology and medicine. [10] In another approach, Jana *et al* utilized FONPs in monitoring of anticancer drug release.[11]

Although organic nanoparticles provide advantages like wider applicability and flexibility in materials synthesis and nanoparticle preparation, advances in this field are rather slow due to several inherent problems associated with their synthesis and isolation.[12-16] It is only in last few years, considerable efforts have been put into the development of new methods to synthesize the FONPs with tuneable size, morphologies, and dispersion. Recent developments in this regard involve synthesis by precipitation[17], dilution of oil-in-water microemulsions in water[18], laser ablation[19], thermal evaporation[20], and reverse microemulsions.[21] Among all these methods, the re-precipitation is one of the simplest and less time consuming method, which has

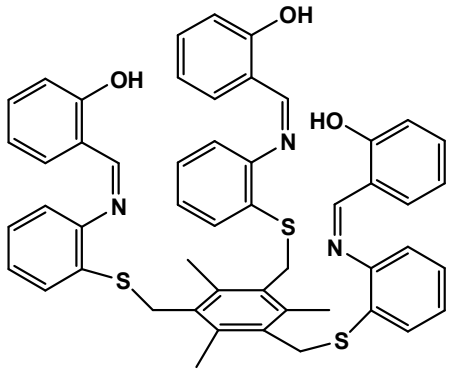

Figure 1. Molecular structure of OTL.

sparked the interest of chemists in the synthesis of FONPs. This method not only facilitates the formation of FONPs but also

enhances the fluorescent quantum yield to many folds.[22-23] FONPs are prepared by simply injecting the non-aqueous solution of organic compound in aqueous phase under vigorous stirring at constant temperature. Aqueous phase insolubility of the organic compound compels the molecules to get aggregate in roughly spherical particles whose size can very well be controlled by the concentration, temperature, and stirring rate.

Herein, we have selected an organic tripodal Schiff base ligand, OTL (Figure 1), to prepare FONPs by reprecipitation method. This is the analogue with slight changes to a molecule with prominent fluorescence properties which demonstrates 'PET' based 'off–on' sensor for Ag^+ recognition.[24] We believe that ONPs of this molecule will have even better photophysical properties which should show size dependent behaviour. Since its analogue has shown specificity towards Ag^+ ions, therefore it opens up a new direction of synthesizing organic– inorganic hybrid nanomaterials by reducing Ag^+ ions on the surface of ONPs. This will allow Ag NPs to grow on the surface of ONPs resulting in the formation of core – shell hybrid morphologies with interesting material properties.[25-27] We can prepare different sizes of ONPs simply by controlling the precursor concentration which will allow us to determine the size dependent photophysical properties. We further plan to exploit their ratiometric recognition of biologically important Cu^{2+} ions in aqueous medium which will allow the possibility to use them as drug release vehicles.

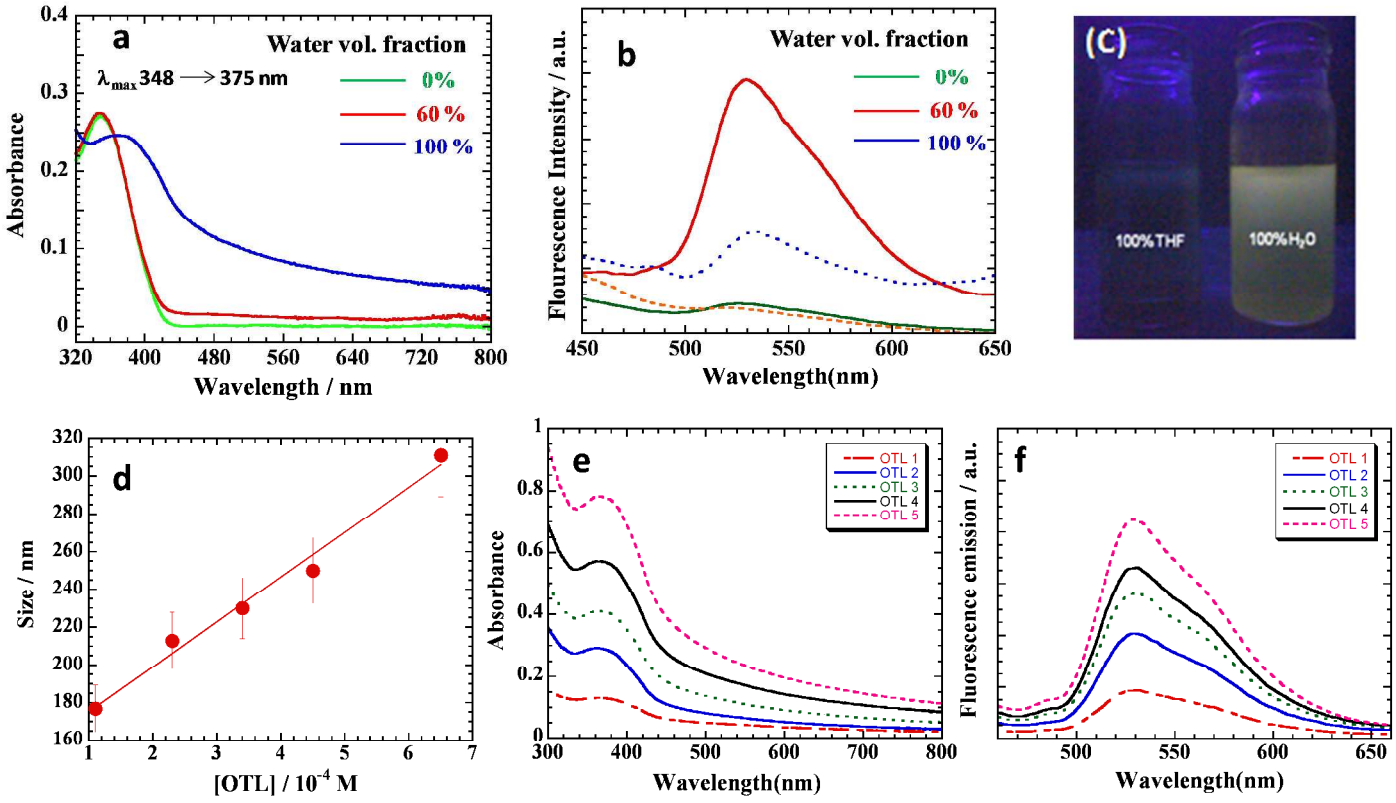

Figure 2. (a) UV-visible, (b) fluorescence spectra of OTL in pure THF, FONPs in pure water, and their mixture. (c) Photographs of FONPs in pure THF and pure water under the effect of UV light. (d) Variation of the size of FONPs with the concentration of OTL as evaluated from DLS measurements, Variation of the (e) UV-visible and (f) fluorescence spectra of FONPs samples of different sizes.

Results and discussion

FONPs

OTL in pure THF shows an absorbance maximum around 348 nm in the UV region due to n-π* transition in -C=N- bond of OTL which red shifts to 375 nm as the amount of water increases and ONPs formation sets in (Figure 2a). It makes the solution slightly turbid with uniform distribution of NPs while no stabilizer such as an appropriate surfactant is required. A prominent red shift in the absorbance happens due to the conformational changes in OTL from the isolated twisted to planar[22] when they are stacked together in an ONP with compact amorphous state. Likewise, their fluorescence emission around 530 nm increases and becomes maximum in pure water (Figure 2b). See a comparison in the fluorescence emission in pure THF and water when exposed to UV (Figure 2c). A little fluorescence in pure THF can be attributed to a rapid non-radiative decay due to the presence of free OTL which may adopt any conformation in contrast to restricted decay when OTL aggregates in the form of FONP in aqueous rich environment and produces radiative decay which makes ONPs fluorescent. DLS analysis provides an estimate of the particle size which increases with the increase in the amount of OTL used (Figure 2d). Thus, a controlled precipitation with predominant non-polar interactions among the larger amount of OTL generates larger NPs. The larger FONPs systematically produce prominent absorbance peaks (Figure 2e) and thus depict the involvement of a stacking arrangement in the FONP format-

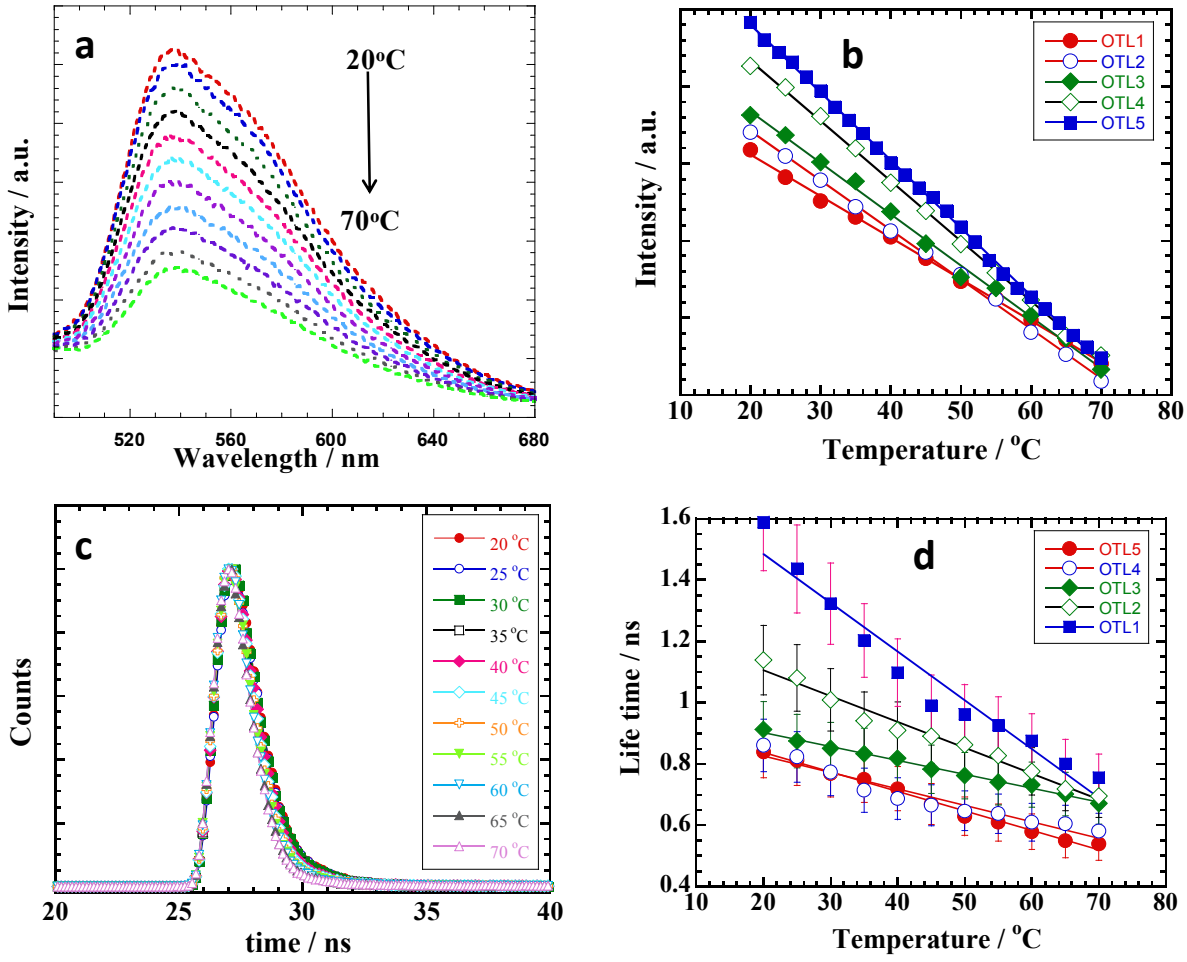

Figure 3. (a) Dependence of the fluorescence intensity of aqueous suspension of FONPs with temperature from 20 – 70 oC. (b) Variation of fluorescence intensity maximum with temperature for FONPs of different sizes. (c) Time resolve fluorescence of aqueous suspension of FONPs with temperature from 20 – 70 °C. (d) Variation of fluorescence life time with temperature for FONPs of different sizes.

-ion. Likewise, fluorescence emission also increased with increase in concentration or increased particle size (Figure 2f). To have better understanding about increased fluorescence intensity the quantum yield was calculated and found to be 0.62, 0.63, 0.60, 0.64, 0.63 for OTL1, OTL2, OTL3, OTL4 and OTL5 respectively. Therefore increase in fluorescence intensity is related only to increased concentration from OLT1-OLT5. Both Fig 2e and f do not show any shift in the absorbance or fluorescence maximum with size which can be attributed to a similar kind of stacking arrangement of OTL molecules in FONPs of different dimensions as well as to their uniform dispersions in aqueous phase. Stacking arrangement of organic molecules in a NP formation can be attributed to the H-type and J-type[28-30] where H-type molecules are aligned parallel to each other with strong intermolecular interactions and are mainly responsible for the non-radiative decay. On the other hand, J-type molecules are arranged in head to tail direction and responsible for the high fluorescence efficiency with bathochromic shift in the UV absorbance. Probably, the latter arrangement is also inducing the fluorescence in the present FONPs. The fluorescence emission of FONPs also closely depends on the temperature variation as well as the size of NPs. Increase in the temperature decreases the fluorescence intensity (Figure 3a). Intensity versus temperature plot for FONPs of different sizes shows a linear dependence on temperature (Figure 3b). In general, fluorescence intensity decreases with increasing temperature due to increased molecular collisions that occur more frequently at higher temperatures especially for species in the solution phase. Collisions deplete energy from the excited state that produces fluorescence and thus convert the radiative decay into a non-radiative decay with the result fluorescence intensity decreases with temperature. Herein, organic molecules (OTL) are already packed in the amorphous FONPs and their packing arrangement in fact made them fluorescence active. That is why, bigger FONPs show greater fluorescence in comparison to the smaller ones (Figure 2f). However, temperature effect demonstrates a more pronounced effect with greater negative slope for bigger FONPs in comparison to the smaller ones (Figure 3b). A linear decrease in the fluorescence intensity with temperature shows that the self quenching of OTL molecules is

proportional to the temperature. Since a larger number of OTL molecules are involved in the formation of bigger ONPs, hence they depict steeper slope in comparison to smaller ONPs. In addition, increase in the temperature induces molecular ordering due to the annealing effects which causes the excited state species

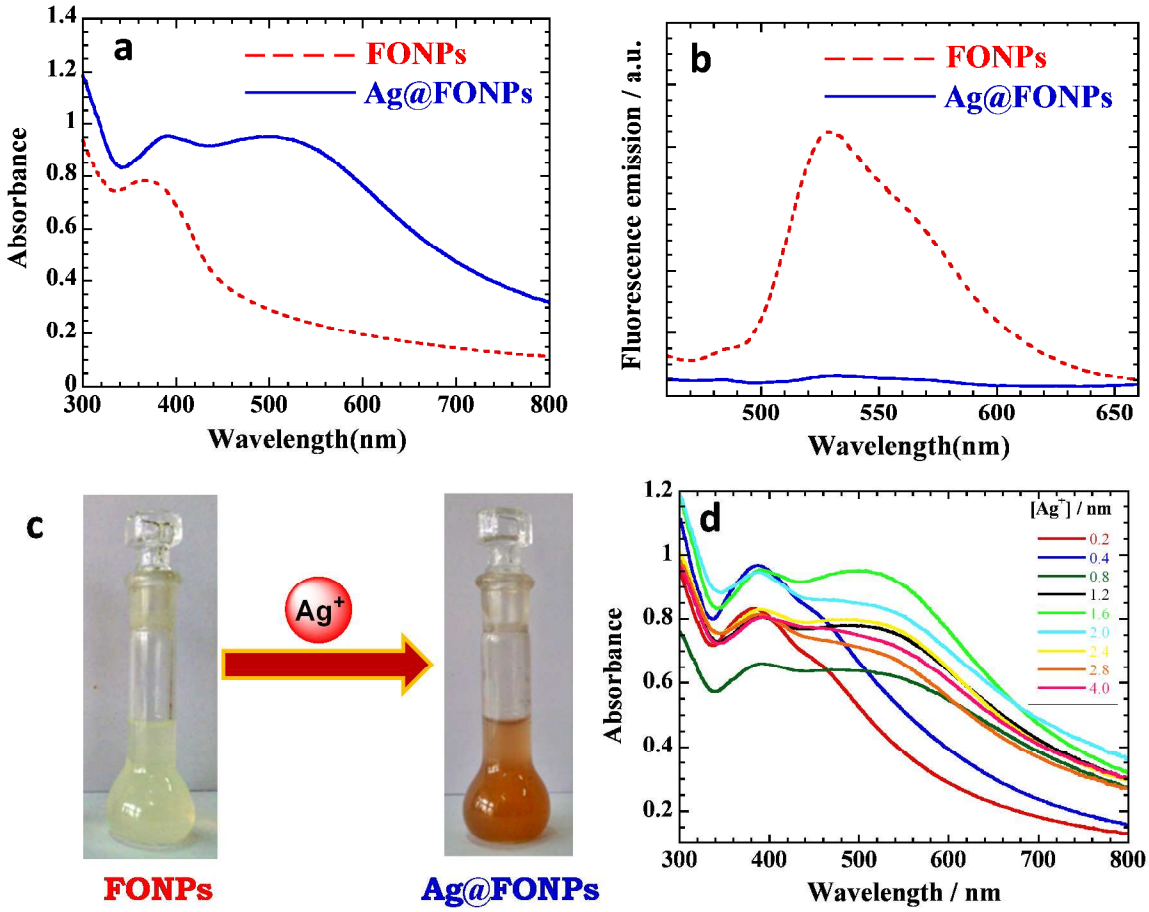

Figure 4. (a) UV-visible, (b) fluorescence spectra of aqueous suspension of FONPs and their corresponding Ag@FONPs and (c) A typical photo of an aqueous suspension of FONPs and dark brown colored aqueous suspension of Ag@FONPs, (d) Variation in the absorbance of FONPs in aqueous suspension in the presence of different concentrations of Ag salt.

to loose their energy through non-radiative decay due to the thermal collisions and thus causing fluorescence quenching. This effect is expected to be more prominent for bigger in comparison to the smaller FONPs. Figure 3c & d shows the lifetime decay profiles at different temperature, which were fit to the multi-exponential function with average lifetime around 1 ns (*see supporting information, Figure S1*). In each case, lifetime decreases with the increase in temperature which was obviously expected in view of the increasing non-radiative decay with temperature. Annealing effect at 75 ^{o}C causes a sufficient phase transformation from amorphous to crystalline and few multiple peaks in a narrow range of $2\Theta \approx 32^{o}$ indicates the growth on {111} crystal planes (*Figure S2*).

Ag@FONPs

The cation binding ability of FONPs in aqueous phase was explored in dilute regimes of various metal nitrate salts (50 μM) in HEPES buffered in DMSO/H_2O (7:3, v/v). Both UV-visible (Figure 4a) as well as fluorescence (Figure 4b) show marked Ag^+ ion recognition behaviour of FONPs. The UV-Visible spectra of FONPs show significant interactions with Ag^+ ions (Figure 4a) and produce another broad band around 500 nm. It results in a dramatic color change of the sample from turbid to sharp brown (Figure 4c) which indicated the formation of Ag NPs because of the reduction of Ag(I) to Ag(0) by OTL. Similar results were reported for the formation of Au NPs in the presence of spherical micelle assemblies of block copolymers.[31-33] Colloidal suspension of tiny Ag NPs produces their characteristic absorbance around 400 nm in the visible region. However, a significant red shift in absorbance of Ag NPs is due to their expected growth on the surface of FONPs due to the selective binding ability of FONPs for Ag^+ ions. Likewise, the emission spectrum of Ag@FONPs completely eliminates the band at 530 nm due to the deactivation of FONPs surface by the growth of Ag NPs. We will further explain the growth of Ag NPs on the surface of FONPs from TEM studies.

^{1}H NMR titrations help us to determine the binding sites of Ag^+ coordination to the receptor pseudo-cavity of organic host (i.e FONP) (Figure S3). Amorphous nature of the FONPs leaves several surface cavities which subsequently become the active

sites for the entrapment of Ag^+ ions and their reduction into tiny Ag NPs. ^1H NMR titrations can help us to investigate this process by varying the mole ratio between Ag^+ and FONPs from 0 to 5 (Figure S3, A – G). A mole ratio of 0.5 (Figure S3, B) induces a shift of $\Delta\delta$ = 0.06 in the signal of –CH=N (8.67 ppm) while aromatic protons (7.54 – 6.82 ppm) also demonstrate a shift of $\Delta\delta$ = 0.02 – 0.07. The shift in –CH=N signal is quite expected as the imine linkage bears the sp^2 nitrogen, which acts as a soft centre for the coordination of soft metal ion like Ag^+. Increase in the mole ratio to 1.5 (Figure S3, D) even shifted the signal of –CH=N up to $\Delta\delta$ = 0.09, with relatively little shift in the aromatic protons. A mole ratio of 2.0 (Figure S3, E) induces split in the signal of –CH=N and merger in the aromatic signals, which were otherwise quite prominent between δ 7.3-7.4 at low mole ratios. The splitting in signals indicates that the organic receptor is not offering the symmetric binding sites from all the three pods to the Ag^+ ions. The solubility profile of both host and metal salt compelled us to use DMSO(d_6) / D_2O solvent system, and the presence of D_2O limits us to follow the –OH signal. However, above titrations demonstrate the most significant role of imine linkages for the formation of metal complex which is further confirmed from the IR measurements in the absence and presence of Ag^+ as depicted in Figure S4. The peaks located at 1641, 1550, 1279 and 1073 cm^{-1} in case of FONPs shift to 1646, 1541, 1283 and 1078 cm^{-1} in the case of Ag@FONPs, respectively. Ag^+ ions have good affinity for electrons and known to bind well with ligands containing lone pair electrons. As good electron donors, both -OH and N of OTL can coordinate with Ag^+ ions to form a stable complexes which induce the red-shift in the IR spectra and is previously reported by other groups as well.[34] In addition, the band for imine linkages originally at 1446 cm^{-1} shows a shift of 5 cm^{-1} which confirms their participation in the complexation with Ag^+ ions. Thus, the collective analysis of NMR and FTIR spectra of OTL and Ag@FONPs clearly demonstrates the interactions of Ag^+ with sp^2 nitrogen atom of –CH=N linkage, which produce no additional signals that could be related to some oxidized species in OTL. This is also not even observed from the IR band due to C=O group or change/cleavage in the structure of OTL. In the light of above results, we purpose the following mechanism for the formation of Ag NPs.

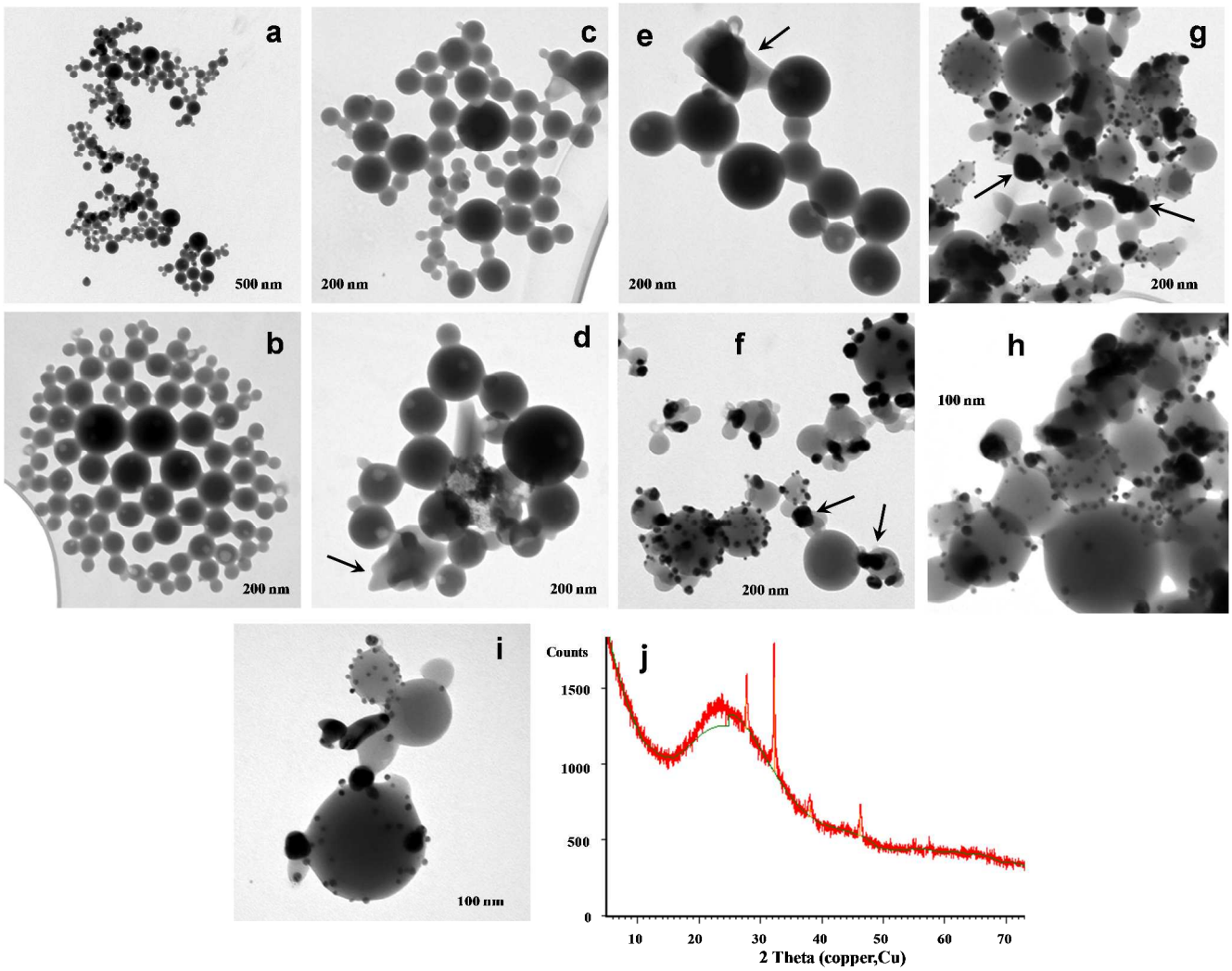

Figure 5. (a) TEM micrographs of fine spherical FONPs made with OTL = 1.1 x 10-4 M in pure water in low resolution. (b) This image shows the budding process of larger NPs into smaller ones, which later on arrange themselves in chain like arrangement (c). Images (d) and (e) show the presence of deformed NPs (indicated by arrows) along with the spherical NPs when FONPs are prepared with OTL = 4.5 x 10-4 M. TEM micrographs (f) and (g) of Ag@FONPs prepared with OTL = 1.1 x 10-4 M and AgNO3 = 0.2 mM. See the growth of Ag NPs as dark dots at the surface of spherical FONPs. Arrows

indicate some of the large size Ag NPs which are produced most probably from the inter – particle fusion of among the smaller ones at the surface of FONPs. Images (h) and (i) depict similar images of Ag@FONPs made with OTL = 4.5 x 10-4 M and AgNO3 = 0.2 mM. (j) XRD patterns of FONPs sample dried at 75 oC demonstrating the fcc crystal structure of Ag NPs.

$$\text{ONPs} + Ag^{+} \xrightarrow{H_2O} Ag(OTL)^{+} \xrightarrow[h\nu]{H_2O} Ag^{0} + \text{OTL}$$

Where OTL ligands on the surface of ONPs first interact with Ag^+ ions through sp^2 hybridised nitrogen atom to form $Ag(OTL)^+$ complex. This complex in the presence of light initiates photoreduction of Ag^+ to Ag^o. Similar type of mechanism has also been proposed by Hada *et al* [35] and Balzani *et al* [36] for the formation of Ag from $Ag(dipy)_2^{2+}$ complex in aqueous solution. Once the nucleating centres are created on the surface of ONPs, they become active sites for subsequent autocatalytic process in the presence of Ag^+ ions and eventually grow into prominent Ag NPs to produce organic – inorganic hybrid morphologies. We will further discuss this point in the light of TEM studies later in the text.

Effect of silver concentration

Growth of Ag NPs on the surface of ONPs is directly related to the amount of the Ag^+ ions reduced into Ag(0) and is closely monitored from the UV-visible behavior. A variation in the concentration of Ag^+ ions from 0.2 mM to 4 mM at constant concentration of FONPs (10 μM) after equilibrating the samples for 12h is depicted in Figure 4d. In the absence of Ag^+ ions, FONPs give characteristic absorbance around 375 nm. However, increase in the amount of Ag^+ produces a new band around 500 nm whose intensity increases up to 1.6 mM, thereafter, it decreases as the concentration further increases. The first increments in the absorbance can be assigned to the increased number of Ag NPs formed on the surface of FONPs which latter on agglomerate to produce larger particles and thus causes a decrease in the absorbance. We will further explain it from the TEM studies.

TEM analysis

TEM studies can help us to evaluate the shape and size of the FONPs as well as the nature of Ag@FONPs hybrid morphologies. Figure 5a shows a low magnification TEM image of small FONPs in the form of fine spheres made from 1.1 x 10^{-4} M of OTL which mostly exist as aggregates in dried state on copper grid. Aggregation happens due to the predominance of the close van der Waal's interactions among the aromatic rings and may be to some extend due to the hydrogen bonding among the hydroxyl groups in the amorphous state. The average size of the spherical FONPs of this sample is close to 175 nm as observed from DLF studies (Figure 2d) though some larger spheres of more than 200 nm are also visible due to the presence of polydisperse behaviour. The later behaviour is the consequence of the budding mechanism which allows the larger aggregates to split into smaller ones as dehydration sets in and is clearly depicted by Figure 5b. Figure 5c shows another typical chain like arrangement of FONPs of the same sample. Such kind of aggregation behaviour is usually demonstrated by the NPs which lack stabilizing agent. A colloidal particle can be properly stabilized in the form of a colloidal sol if an appropriate amphiphilic stabilizing agent like surfactant is used. Since in the presence study, we focus on the synthesis and properties of FONPs, therefore we preferred not to use any surfactant which might impede their fluorescence behavior. Further increase in the concentration of OTL to 4.5 x 10^{-4} M increases the size of the FONPs around 250 nm as depicted by the DLS studies in Figure 2d which suggests a good correlation between the DLS and TEM studies. However, increase in the concentration also induces the deformation in the spherical shape. See the deformed NPs indicated by the black arrows in Figure 5d and 5e. The number of deformed FONPs is much less in comparison to spherical and there is no marked effect on the overall fluorescence behavior of FONPs. As FONPs specifically bind to Ag^+ ions as depicted in Figure 4 & 5, TEM analysis demonstrate the growth and formation of small Ag NPs on the surface of FONPs. Figure 5f and 5g show TEM micrographs of Ag@FONPs of the sample of Fig 5a-c. Both images show several small black Ag NPs of 5 – 10 nm grown on the spherical FONPs. A much darker contrast of the Ag NPs in comparison to that of FONPs is simply due to their metallic nature which causes much greater diffraction. Black arrows indicate some larger Ag NPs in comparison to several smaller ones. It seems that they are the result of inter-particle fusion among the smaller Ag NPs when they happen to grow in close vicinity of each other. Figure 5h and 5i show the images of Ag@FONPs of sample of Figure 5d,e with larger size in comparison to the previous sample. Again, small Ag NPs grown on the surface of FONPs are clearly visible. XRD patterns show a fine fcc crystalline geometry of Ag with prominent peaks at 27.7°, 32.2°, 38.0°, and 46.2° (Figure 5j). The images also demonstrate that no independent Ag NPs exist in the solution and the surface of the FONPs constituted by the J-type packing arrangement of OTL molecules is responsible for the reduction of Ag(I) into Ag(0) with the consequence Ag NPs only grow on the surface of FONPs. Thus, the growth of the Ag NPs in fact impedes the absorption as well as the radiative decay of FONPs as depicted in Figure 4a and b, respectively, which happens due to the quenching effects. TEM images were also recoded after dissolving the organic matter in THF/H_2O. Slightly agglomerated Ag nanoparticles were clearly observed which were earlier adsorbed on the surface FONPs (*Figure S5*).

Application of FONPs in Ag extraction and Cu recognition

Formation of Ag@FONPs (Figure 6ai) suggests that FONPs can be repeatedly used for the extraction of Ag^+ ions from aqueous samples with the ability of FONPs to work for any given number of times. In order to demonstrate it, we dissolved Ag@FONPs in THF/H_2O (8:2, v/v) mixture that produced sharp yellow colored solution (Figure 6aii) due to tiny Ag NPs. Because of the favorable solubility of FONPs in THF/H_2O (8:2, v/v), the solution is practically left with the colloidal suspension of Ag NPs which can be easily extracted from the solution by centrifugation. The remaining transparent solution (Figure 6aiii) containing mainly soluble OTL can further be used for the formation of FONPs by increasing the amount of water and hence can be repeated used for the same purpose.

Likewise, Ag@FONPs can be used as sensors for metal ions and

anions recognition. A change in the absorption profile of Ag@FONPs dissolved in aqueous THF (8:2, v/v) upon addition of a particular metal ion (50 μM) in HEPES buffered DMF/H_2O (8:2, v/v) gives direct evidence of the binding behaviour (Figure 6b). The addition of Cu^{2+} resulted into a significant change in the absorption spectrum of FONPs**.** The binding of FONPs to Cu^{2+} furnished a new band at 421 nm. The addition of any other metal ion (*i.e.* K^+, Mg^{2+}, Ca^{2+}, Ba^{2+}, Sr^{2+}, Mn^{2+}, Ni^{2+}, Co^{2+}, and Zn^{2+}) showed no such significant binding. The sensing of Cu^{2+} is of immense importance because Cu^{2+} is third most abundance transition metal in human body. It play significant role in various physiological processes ranging from hemoglobin biosynthesis to nerve function regulation.[37-39] The excessive use of copper due to

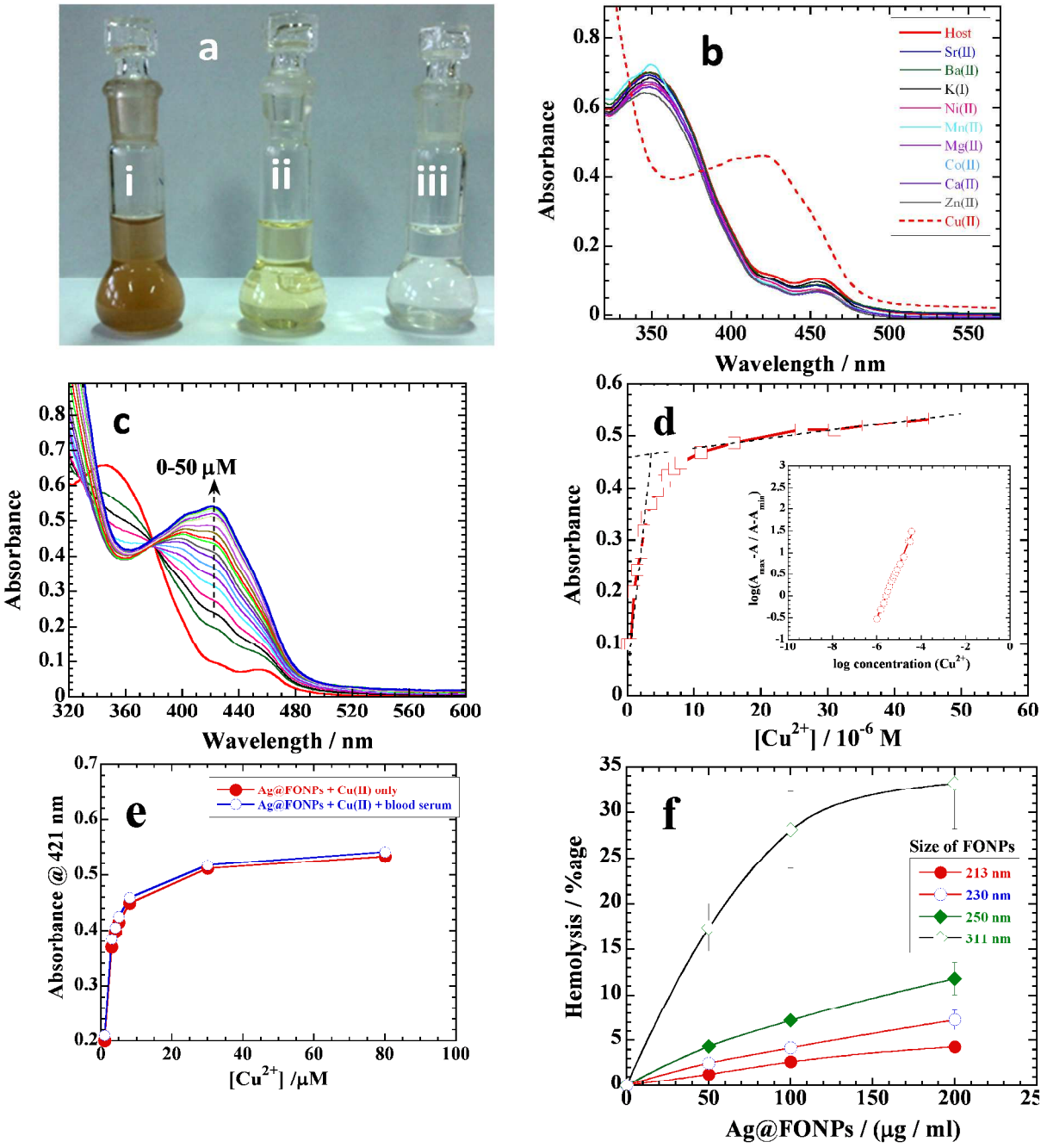

Figure 6. Photographs of (ai) aqueous suspension of Ag@FONPs, (aii) Ag NPs in THF + water mixture, and (aiii) the solution after extraction of Ag NPs. See details in the text. (b) UV-visible absorbance of Ag@FONPs in the presence of various ions. (c) A variation in the UV-visible absorbance of Ag@FONPs in the presence of varying amounts of Cu^{2+} ions. (d) A variation in the intensity of absorbance of Cu^{2+} complex with the amount of Cu^{2+} ions, and it is compared in (e) in blood serum. (f) Variation of percentage hemolysis with the amount of Ag@FONPs for NPs of different sizes.

its applications in industrial, pharmaceutical and agricultural purposes led to serious threat to environment and human health.[40,41] The misregulation of Cu^{2+} is related to many diseases such as Alzheimer's, Prion, Menkes, and Wilson diseases, lipid

metabolism, and inflammatory disorders.[42,43] These diverse applications of Cu^{2+} have led to a strong interest in the development of selective Cu^{2+} probes.[44-47] To gain more insight into the Cu^{2+} recognition behavior, titration of Ag@FONPs dissolved in aqueous THF (8:2, v/v) with Cu^{2+} was performed (Figure 6c). A successive increase in the amount (0 - 50μM) of Cu^{2+} results in a continuous reduction of absorbance at 350 nm and simultaneous increase in absorbance at 421 nm with one isobestic point at 376 nm (Figure 6c). The detection Limit (LOD) was measured to be 0.24 μM. The linear range is observed between 0 – 4 μM concentration of Cu^{2+} (*Figure S6*). To test the practical applicability of Ag@FONPs as a Cu^{2+} selective chromogenic sensor; the interference of other metal ion in sensing of Cu^{2+} by Ag@FONPs was studied. Competitive experiments were carried out in the presence of Cu^{2+} (50 equiv.) mixed with one of K^+, Ca^{2+}, Mg^{2+}, Ba^{2+}, Sr^{2+}, Mn^{2+}, Co^{2+}, Ni^{2+}, Zn^{2+} (50 equiv.). As shown in *Figure S7*, no significant variation in the intensity was found by comparing the profile with and without the other metal ions, which means that Ag@FONPs dissolved in aqueous THF (8:2, v/v) can selectively sense the Cu^{2+} at μM level. Fig 6d demonstrates the complete saturation of all binding sites on the surface of Ag@FONPs by 4 μM Cu^{2+} that provides about 1:25 mole ratio between the OTL and Cu^{2+}. It is possible to calculate the binding constant of Cu^{2+} ions with OTL by using log $[A_{max} - A]/[A - A_{min}]$ = -log $[Cu^{2+}]$- log β (where A_{max} and A_{min} are the maximum and minimum absorbance, A is the measured absorbance, and β represents the binding constant) equation previously used by other authors[48] for the related systems. Inset shows the application of this relation on the data of Figure 6d, which gave the binding constant = 6.9. In addition, a variation in the pH did not show any marked effect on the absorption profile of Ag@FONPs (*Figure S8*) and hence it can be utilized in a wide pH range. There is no effect on the stability of Ag@FONPs in the absence and presence of Cu^{2+} ions. This has been determined by using EDTA, the presence of which diminishes the peak observed at 421 nm and eventually generated a spectrum similar to that before the addition of Cu^{2+} ions (*Figure S9*). Also the UV-Vis spectral changes were observed on addition of Cu^{2+} ions to Ag@FONPs solution as function of time for period ten days. No significant changes were observed as shown in *Figure S10*. Hence, it concludes that AgNP@FONPs are quite stable before and after interaction with Cu^{2+} ions. Ag@FONPs also does not show any selectivity against Cu^{+} (*Figure S11*).

The observed binding affinity of Ag@FONPs for Cu^{2+} is the consequence of unique combination of sulfur and sp^2 nitrogen donor sites of FONPs. These types of binding sites are also prevailed in the naturally occurring copper proteins, highlighting the importance of these binding sites to constitute the optimum coordination spheres in terms of compatibility between host and guest[49]. Thus, the binding sites of FONPs act as receptor subunits for Cu^{2+} ions and the occurrence of such kind of host – guest process in the vicinity of Ag NPs causes modulation in the photophysical properties of Ag NPs thereby allowing them to act as signaling subunit of sensor assembly. In addition, above mentioned NMR studies also indicated the presence of unsymmetrical binding of tripodal ligand through three binding pods to Ag^+ which means that all binding sites are not engaged in association with Ag^+ ion, and hence there is equal probability of free binding sites to interact with Cu^{2+} ions. Unfortunately, this association is not clearly depicted by the emission spectroscopy because the fluorescence emission of ONPs has already been quenched by the interactions with Ag^+ ions and its subsequent formation of Ag@FONPs. Therefore, no marked changes are observed in the fluorescence spectrum of AgNP@FONPs in the presence of Cu^{2+} or other metal ions or anions (*Figure S12*). In addition, the binding affinity of Ag@FONPs to bind Cu^{2+} also works very well in biological systems (*Figure S13*), where no change in the binding affinity from the absorption spectra of Ag@FONPs in the presence as well as in the absence of blood serum is observed (Figure 6e). This shows that Ag@FONPs are highly specific towards the Cu^{2+} ions even in the presence of much complex biological environment. Taking advantage of this observation, we further tried to understand the hemolytic ability of Ag@FONPs so as to explore their potential as drug delivery vehicles in the systemic circulation. Hemolytic assay of four samples of Ag@FONPs has been presented in Figure 6f along with the sample photos of 230 nm Ag@FONPs and corresponding absorbances (*Figure S14*). Smallest Ag@FONPs (i.e. 213 nm) show least hemolysis and it remains less than 5 % even up to 200 μg/ml, while it increases with the increase in the size of the NPs. Similar hemolytic behavior on the basis of the size of the NPs has already been reported by other authors.[50-52] As depicted in the TEM images (Figure 5), the surface of Ag@FONPs is mainly occupied by the tiny Ag NPs which are considered to be the active sites for interactions with cell membrane of red blood cells because charged surfaces have greater potential to interact and rupture the cell membranes.[53,54] Thus, larger size of Ag@FONPs is expected to induce greater hemolysis than the smaller ones. Therefore, smaller NPs of ~ 200 nm with minimum hemolysis can be used as vehicles of drug release in systemic circulation. Additionally, we tried to evaluate the biocompatibility of Ag@FONPs with living cells and performed the MTT assay with osteosarcoma cancer cell line under standard conditions (incubation at 37 ^oC for 2 days in CO_2 atmosphere, 5%). Ag@FONPs of largest size (311 nm) show the cell viability as high as 82 %, thus Ag@FONPs of smaller size are much better vehicles for drug release as indicated above from the haemolytic assay.

Concluding remarks

We demonstrate a simple method for the synthesis of fine spherical FONPs by using a OTL in aqueous phase. OTL itself is not a fluorescent molecule but shows radiative emission when it aggregates in a specific order in amorphous nanoparticle whose emission increases with the increase in the size and decreases with the rise in temperature. Because of its specific Ag^+ ions binding ability, FONPs also show the same property and possess an ability to reduce Ag(I) into Ag(0) resulting in the growth of Ag NPs on the surface of FONPs to produce organic – inorganic hybrid nanoparticles. Ag@FONPs are not fluorescent due to the quenching of fluorescence emission of FONPs when Ag NPs grow on their surface. However, Ag@FONPs are the fine chromogenic agents for the detection of Cu^{2+} even in the presence of blood serum and hence can be used in the biological systems. Apart from this, NPs of ~ 200 nm show little hemolysis up to 200 μg/ml, thus making them suitable vehicles for the drug release in systemic circulation.

Experimental

Materials

All chemicals were obtained from Sigma and used as received without further purification. The organic tripodal Schiff base (Figure 1) was synthesized as reported earlier.[55] Syntheses of receptors

Synthesis of FONPs and Ag@FONPs

The FONPs were synthesized by reprecipition method.[56] Breifly, 1 mL of OTL solution in tetrahydrofuran was injected with microsyringe at a constant rate to double distilled water (50 mL) under vigorous stirring. The solution was then sonicated for 20 min at constant temperature to produce FONPs of desired size which provided a slight turbidity with greenish ting (Figure 4c). The size of FONPs was simply controlled by varying the concentration of OTL in the solution. Organic – inorganic hybrid Ag@FONPs were prepared by taking an aqueous suspension of FONPs of desired concentration along with 0.2 mM of $AgNO_3$. Heating this solution at constant temperature of 70 ^oC initiated the reduction of Ag(I) into Ag(0) resulting in the formation of Ag NPs covalently attached to the surface of FONPs through sulfur linkages. The color of the final suspension was shinning brown indicating the formation of Ag@FONPs (Figure 4c).

Methods

UV-Visible absorption spectra of FONPs suspensions were recorded on Specord 250 Plus Analytik jena spectrometer. Steady state and time resolved fluorescence spectroscopy of ONPs suspensions were carried out by using PTI QuantaMaster and PicoMaster 2 TCSPC Lifetime Fluorometer, respectively. Both instruments were equipped with a thermoelectrically temperature controlled cell holder that allowed to measure the spectrum at a constant temperature within ± 1 ^oC. In order to obtain the fluorescence lifetime, the profile of instrument response function (IRF) (excitation pulse) has been measured in addition to the fluorescence decay. In a typical experiment, two curves are measured: the IRF using a scatterer solution and the decay curve (*see supporting information, Fig S1a*). Analysis is then performed by convoluting the IRF with a model function (e.g. a single exponential decay or a double exponential decay or some other function) and then comparing the result with the experimental decay. This is done by an iterative numerical procedure until the best agreement with the experimental decay curve is achieved. ^1H spectra were recorded in DMSO-d_6 on a JEOL II 400 spectrometer (400 MHz with TMS as internal standard; chemical shifts are expressed in ppm). FT IR spectra were recorded on a Bruker Tensor 27 spectrometer in the form of liquid samples. The PANalytical X'PERT PRO diffractometer was used for X-ray diffraction (XRD) with a scan speed of 10^o/min for 2θ in a range from 10 to 80 (45 KV, 40 mA using Ni-filtered Cu K_α radiations). Transmission Electron Microscopic (TEM) analysis was done on a JEOL 2010F at an operating voltage of 200 kV. The samples were prepared by mounting a drop of a solution on a carbon coated Cu grid and allowed to dry in the air. The particle size of FONPs and AgNP@FONPs were measured by using external probe feature of Metrohm Microtrac Ultra Nanotrac Particle Size Analyzer (Dynamic Light Scattering).

Acknowledgment

This work is supported by CSIR, New Delhi, [01(2417)/10/EMR-11]. A. S. thanks CSIR for a fellowship. G. K. thankfully acknowledges the financial support provided by the Research and Development Council (RDC) of Newfoundland and Labrador, NSERC, and the Office of Applied Research at CNA.

Notes and references

[a]*Department of Chemistry, Indian Institute of Technology Ropar (IIT Ropar), Rupnagar, Panjab, India, 140001, Tel: 91- 1881242176, E-mail: nsingh@iitrpr.ac.in*
bDepartment of Physics, College of The North Atlantic, Labrador City, Canada. cDepartment of Chemistry, Wilfrid Laurier University, Science Building, Waterloo, Canada; E-mail: ms_bakshi@yahoo.com

† Electronic Supplementary Information (ESI) available: UV–vis absorption spectra.See DOI: 10.1039/b000000x/

References

1 S.J. Lim, B.K. An, S.D. Jung, M.A. Chung, S.Y. Park, Angew. Chem. Int. Ed., 2004, 43, 6346–6350.
2 Y.-Y. Sun, J.-H. Liao, J.-M. Fang, P.-T. Chou, C.-H. Shen, C.-W. Hsu, L.-C. Chen, *Org. Lett.,* **2006**, *8*, 3713-3716.
3 B.-K. An, S.-K. Kwon, S. Park, *Angew. Chem. Int. Ed.*, **2007***, 46*, 1978-1982.
4 R. Abbel, R. van der Weegen, E. W. Meijer, A.P. H. J. Schenning, *Chem. Commun*., **2009**, 1697–1699.
5 X. Sheng, Y. Qian, *J. Nanosci. Nanotechnol.*, **2010,** *10*, 8307-8311.
6 H.B. Li, H.J. Yan, *J. Phys. Chem. C* **2009**, *113*, 7526-7530.
7 H. Li, J. Xu, H. Yan, *Sens. Actuators B* **2009**, *139*, 483-487.
8 H.-J. Kim, J. Lee, T.-H. Kim, T.S. Lee, J. Kim, *Adv. Mater.,* **2008**, *20*, 1117–1121**.**
9 H. H. Lin, S.Y. Su, C.C. Chang, *Org. Biomol. Chem.* **2009**, *7*, 2036-2039.
10 K. Petkau, A. Kaeser, I. Fischer, L. Brunsveld, A.P.H.J. Schenning, *J. Am. Chem. Soc.*, **2011**, *133*, 17063-17071.
11 A. Jana, K. Sanjana, P. Devi, T.K. Maiti, N.D.S. Pradeep, *J. Am. Chem. Soc.*, **2012**, *134*, 7656–7659.
12 M. Kumar, S.J. George, *Nanoscale*, **2011**, *3*, 2130-2133.
13 T.O. McDonald, P. Martin, J.P. Patterson, D. Smith, M. Giardiello, M. Marcello, V. See, R. K. O'Reilly, A. Owen, S. Rannard, *Adv. Funct. Mater.* **2012**, *22*, 2469–2478.
14 X. Zhang, S. Wang, L. Xu, L. Feng, Y. Ji, L. Tao, S. Li, Y. Wei, *Nanoscale*, **2012**, *4*, 5581-5584.
15 F.G. Qu, J.A. Liu, H.J. Yan, L.F. Peng, H.B. Li, *Tetrahedron Lett.* **2008**, *49*, 7438–7441.
16 E. Bilgili, J. Yepes, B. Scarlett, B. *Chem. Eng. Sci.* **2006**, *61*, 149.
17 L. Kang, Y. Chen, D. Xiao, A. Peng, F. Shen, X. Kuang, H. Fu, J. Yao, *Chem. Commun*., **2007**, 2695-2697.
18 F. Ozer, M.O. Beskardes, E. Piskin, *J. Appl. Polym. Sci.*, **2000**, *78*, 569-575.
19 Y. Tamaki, T. Asahi, H. Masuhara, H. *J. Phys. Chem. A,* **2002**, *106*, 2135-2139.
20 J.J. Chiu, C.C. Kei, T.P. Perng, W.S. Wang, *Adv. Mater.*, **2003**, *15*, 1361-1364.
21 S. Magdassi, M.B. Moshe, *Langmuir*, **2003**, *19*, 939-942.
22 B.K. An, S.K. Kwon, S.D. Jung, S.Y.; Park, *J. Am. Chem. Soc.*, **2002**, *124*, 14410-14415.
23 B.K. An, J. Gierschner, S.Y. Park, *Acc. Chem. Res.*, **2012**, *45*, 544-554.
24 V.K. Bhardwaj, A.P.S. Pannu, N. Singh, M.S. Hundal, G. Hundal, *Tetrahedron*, **2008**, *64*, 5384-5391.
25 Z. Markova, A.B. Bourlinos, K. Safarova, K. Polakova, J. Tucek, I. Medrik, K. Siskova, J. Petr, M. Krysmann, E.P. Giannelis, R. Zboril, *J. Mater. Chem.*, **2012**, *22*, 16219-16223.
26 Q. Song, Z.J. Zhang, *J. Am. Chem. Soc.*, **2012**, *134*, 10182-10190.

27 P. Podsiadlo, S.G. Kwon, B. Koo, B. Lee, V.B. Prakapenka, P. Dera, K.K. Zhuravlev, G. Krylova, E.V. Shevchenko, *J. Am. Chem. Soc.* **2013,** *135***,** 2435-2438.

28 S. Yagai, Y. Goto, X. Lin, T. Karatsu, A. Kitamura, D. Kuzuhara, H. Yamada, Y. Kikkawa, A. Saeki, S. Seki, *Angew. Chem. Int. Ed.*, **2012**, *51*, 6643-6647.

29 S. Yagai, K. Iwai, T. Karatsu, A. Kitamura, *Angew. Chem. Int. Ed*., **2012**, *51*, 6643-6647.

30 K. Misawa, T. Kobayashi, *Hierarchical Structure in Oriented J-aggregates. In J-Aggregates* (Eds.: T. Kobayashi), World Scientific Publishing, Singapore, 1996.

31 P. Khullar, V. Singh, A. Mahal, H. Kumar, G. Kaur, M.S. Bakshi, *J. Phys. Chem. B*, **2013**, *117***,** 3028 - 3039.

32 P. Khullar, V. Singh, A. Mahal, H. Kaur, T.S. Banipal, G. Kaur, M.S. Bakshi, *J. Phys. Chem. C*, **2011**, *115*, 10442-10454.

33 P. Khullar, A. Mahal, V. Singh, T.S. Banipal, G. Kaur, M.S. Bakshi, *Langmuir* **2010**, *26*, 11363-11371.

34 Q. Li, B. Sun, I.A. Kinloch, D. Zhi, H. Sirringhaus, A.H. Windle, *Chem. Mater*., **2006**, *18*, 164–168.

35 E.L. Que, D.W. Domaille, C.J. Chang, *Chem. Rev.,* **2008**, *108*, 1517-1549.

36 H. Hada, Y. Yonezawa, A. Yoshida, A. J. Kurakake, *J. Phy. Chem.* **1976,** *80*, 2728-2731.

37 V. Balzani, A. Bertoluzza, V. Carassiti, *Bull. Soc. Chim. Belg*., **1962**, *71*, 821-830.

38 E.D. Harris, *J. Trace Elem. Exp. Med.*, **2001***, 14*, 207-210.

39 W. Schmidt, M. Bartels, J. Tittel, C. Fühner, *New Phytol.*, **1997**, *135*, 659-666.

40 I.A. Koval, P. Gamez, C. Belle, K. Selmeczi, J. Reedijk, *Chem. Soc. Rev.*, **2006**, *35*, 814-840.

41 S.L. Belli, A. Zirino, *Anal. Chem.*, **1993**, *65*, 2583-2589.

42 K.J. Barnham, C.L. Masters, A.I. Bush, *Nat. Rev. Drug Discov.*, **2004**, *3*, 205-214.

43 E. Gaggelli, H. Kozlowski, D. Valensin, G. Valensin, *Chem. Rev*., **2006**, *106*, 1995-2044.

44 S. Sarkar, S. Roy, A.Sikdar, R.N. Saha, S.S. Panja, *Analyst*, **2013**, *138*, 7119-7126.

45 Y. Zhou, S. Wang, K. Zhang, X. Jiang, *Angew. Chem.*, **2008***, 47*, 7454-7456.

46 H.-H. Wang, L. Xue, Z.-J. Fang, G.-P. Li, H.A. Jiang, *New J. Chem*., **2010**, *34*, 1239-1242.

47 M.-C. Lu, L.-Y. Chiu, L.-Y. Chiu, C.-Y. Lin, J.-C. Horng, *Anal. Methods*, **2013,** *5*, 1702-1707.

48 A. P. de Silva, H. Q. N. Gunaratne, *Chem. Commun.* **1990***,* 186–187.

49 B. G. Malmstrom, *Eur. J. Biochem*., **1994**, *223*, 711-718.

50 H. Zhang, D.R. Dunphy, X. Jiang, H. Meng, B. Sun, D. Tarn, M. Xue, X. Wang, S. Lin, Z. Ji, R. Li, F.L. Garcia, J. Yang, M.L. Kirk, T. Xia, J.I. Zink, A. Nel, C.J. Brinker, *J. Am. Chem. Soc.*, **2012,** *134,* 15790-15804.

51 J.M. Shen, X.M. Guan, X.Y. Liu, J.F. Lan, T. Cheng, H.X. Zhang, Bioconjugate Chem., **2012,** *23*, 1010-1021.

52 T. Asefa, Z. Tao, *Chem. Res. Toxicol.*, **2012,** *25,* 2265-2284.

53 P. Khullar, V. Singh, A. Mahal, P.N. Dave, S. Thakur, G. Kaur, J. Singh, S. Kamboj, M. S. Bakshi, *J. Phy.Chem.C*, **2012,** *116,* 8834-8843.

54 A. Mahal, P. Khullar, H. Kumar, G. Kaur, N. Singh, M. Jelokhani-Niaraki, M.S. Bakshi, *ACS Sustainable Chem. Eng.*, **2013,** *1,* 627-639.

55 N. Singh, M. Singh, M.S. Hundal, G. Hundala, M. Martinez-Ripoll, *Tetrahedron*, **2005**, *61*, 7796-7806.

56 R.O. Al-Kaysi, A.M. Müller, T.S. Ahn, S. Lee, C.J. Bardeen, *Langmuir*, **2005**, *21*, 7990-7994.

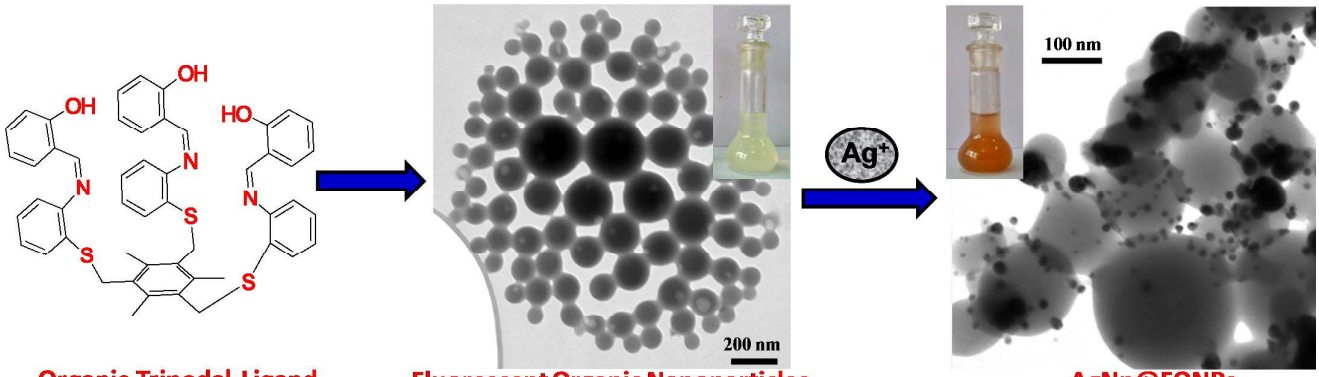

An organic-inorganic nanohybrid material is prepared for chemosensor development in aqueous medium.